INITIAL COMMISSIONING SIMULATIONS FOR THE DIAMOND-II BOOSTER

D. Rabusov*, I. P. S. Martin, Diamond Light Source, Oxfordshire, UK

Abstract

The Diamond-II booster ring is designed to reduce the emittance and the bunch length for efficient injection into the storage ring. Non-optimal commissioning of the injector might increase the dark-time period and the impact on the existing scientific program. This work explores the strategies for booster commissioning to predict and resolve possible issues. The results include tracking simulations with realistic errors such as alignment of magnets and precision of beam diagnostic devices, errors in the magnet gradients, eddy-current effects, measured multipole errors in magnets, and pulsed-magnet time jitter.

INTRODUCTION

Efficient injection into the Diamond-II storage ring requires the upgrade of the existing booster [1]. This work analyses the performance of the booster during the energy ramp in terms of its robustness to errors such as misalignments, field errors, eddy currents and undesirable multipoles in the magnets. Previously, the initial steps towards setting up the commissioning simulations for the Diamond-II booster ring were carried out in *ELEGANT* [2]. This work demonstrates the progress towards the transition to *AT2* [3] to match with the storage ring studies and simplify the development and testing of online Matlab commissioning tools.

ANALYSIS OF BOOSTER MAGNET DATA

Measured multipole components in the pre-series booster quadrupole and sextupole magnets were provided by the Supplier, Danfysik. The datasets include the measurements performed before and after the reassembly of magnets. In this work, we follow the same procedure as described in Ref. [1] to characterise the dynamic aperture at a fixed energy. However, the main B-field as well as the reference gradients in the booster magnets follow the energy-ramp waveform, and the higher-order multipoles scale accordingly. To take this into account, the pre-series measured data has been extrapolated to match the reference gradients of the quadrupoles and sextupoles at any given energy point. Another obstacle is that the available pre-series data contains only one example magnet for each magnet type. The errors have been added to the model as systematic or random. The model setup includes single-particle tracking for 256 turns and averaging over 20 error seeds. The results below include multipole errors in quadrupoles and sextupoles up to the 17-th order.

The results of the dynamic-aperture characterisation from particle tracking are summarised in Fig. 1, in this case, multipole errors are considered to be systematic. The four panels show the dynamic aperture at fixed energies during the ramp, the energy points are chosen as the injection energy 100 MeV, the point at which the trim sextupole gradient b_3 correcting for eddy currents is the strongest $E = 200$ MeV, then $E = 2.16$ GeV when $b_3 B\rho$ in the trim sextupoles is largest; and the extraction energy 3.5 GeV. The black, blue and red curves correspond to the dynamic apertures without multipole errors, with errors measured before the magnet reassembly, and with the errors measured after the magnet reassembly respectively. The orange curve indicates the physical aperture corresponding to the vacuum chamber.

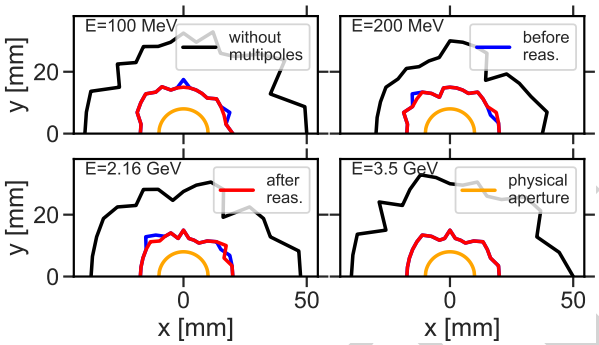

Figure 1: Dynamic aperture throughout the energy ramp. Multipole errors in quadrupoles and sextupoles added as a systematic error.

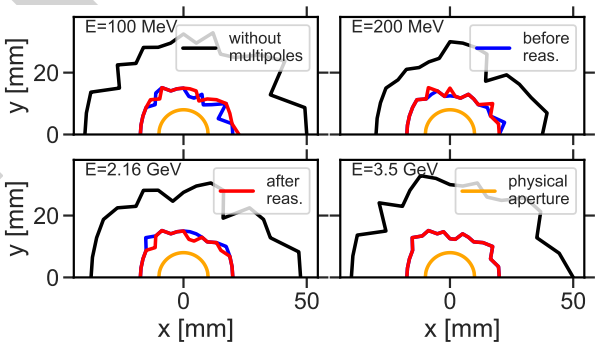

Figure 2: Dynamic aperture throughout the energy ramp. Multipole errors in quadrupoles and sextupoles added as a random error.

Similarly to Fig. 1, the black, blue and red curves in Fig. 2 represent the dynamic apertures without and with the multipoles before and after magnet reassembly. In this case, the errors are added as random components with the measured values being taken as one sigma of a normal distribution truncated at two sigmas. The results of Figs. 1 and 2 suggest that the dynamic aperture reduces when the model includes multipole errors in quadrupoles and sextupoles. However, the dynamic aperture remains larger than the physical aperture

* dmitrii.rabusov@diamond.ac.uk

throughout the ramp. Additionally, the main field components for the normal, focussing and defocussing prototype dipoles have been assessed and found to be acceptable.

ENERGY RAMP

Next, it is important to create a simulation setup with synchrotron-radiation effects for particle tracking throughout the ramp. A pass method *BndMPoleSymplectic4RadPass* is used to take radiation damping into account. Then, two options for the quantum excitation were tested, using a separate element, *qdifElemAT* [3], or a pass method *BndMPoleSymplectic4QuantPass*. Both approaches provide similar results.

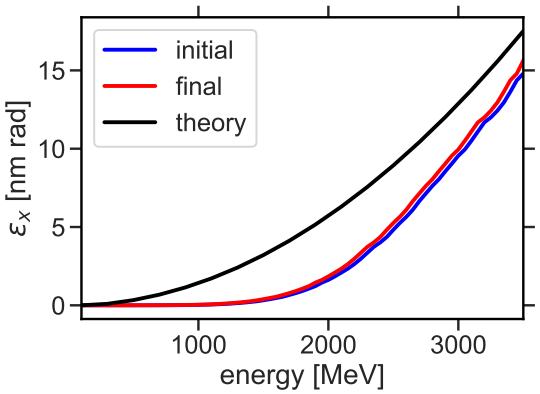

Figure 3: Horizontal emittance in the Diamond-II booster ring throughout the ramp using a matched beam at the injection energy.

Figure 3 demonstrates the results of particle tracking of a beam matched to the injection optics. The quantum excitation is implemented by using the quantum-diffusion element. Tracking is done in fixed-energy steps with 1024 turns at each energy point, using the final beam distribution at the previous step as an initial beam distribution for the next step. The beam distribution was represented by 1024 particles. The blue and red curves correspond to the initial and final horizontal emittance at each energy step, whereas the black curve represents the theoretical ('Ohmi') horizontal emittance at a given energy.

Synchronisation of Dipole Magnets

The power supplies for the booster bending magnets are likely to have systematic timing errors. This can result in an energy-dependent orbit distortion. In the case of a combined-function bending magnet, the timing error also perturbs betatron tunes and chromaticity. This timing error was implemented in AT2 using

$$\frac{\Delta B}{B\rho} = \left[\frac{E_{\max}}{E\,(1+\kappa)}\left(\kappa - \cos(2\pi f_{\mathrm{rep}}(t+t_{\mathrm{lag}}))\right) - 1\right]\frac{1}{\rho_0}, \quad (1)$$

where $\kappa = (E_{\max} + E_{\min})/(E_{\max} + E_{\min})$, ρ_0 is the nominal bending radius, $f_{\mathrm{rep}} = 5$ Hz is the repetition rate, t_{lag} is the timing error. There are three families of bending magnets in the Diamond-II booster ring including the normal dipoles, the defocussing dipoles and the focussing dipoles. All three magnet types are expected to have timing errors of up to 100 microseconds (systematic).

Figure 4 shows an example scenario where the error in the normal dipole is -106.83 µs, in the defocussing dipole it is -47.44 µs and in the focussing dipole it is 57.05 µs. The closed orbit is dominated by the error in the normal dipoles.

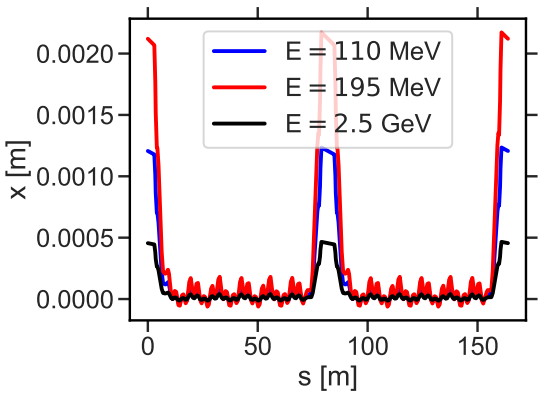

Figure 4: Horizontal orbit at three energies during the ramp assuming systematic timing errors for each family of dipole.

The error in the dipole magnets is strongest at ≈195 MeV, which is represented by the red curve in Fig. 4. For comparison, the blue and black curves represent the closed orbit at lower and higher energies respectively. There are four normal dipoles in the booster ring; one is in the beginning of the lattice, two of them are located in the middle of the ring, and the last normal dipole can be found at the end of the ring. The errors result in two closed-orbit bumps in the high-beta straight sections, which can be measured by four BPMs located between the normal dipoles.

Next, it is important to find a robust correction scheme which can minimise the synchronisation error between the dipole power supplies. The idea is to use an orbit-response matrix by deliberately setting the dipoles to have an offset of 10 microseconds and recording the orbit at 195 MeV. This will require 6 full booster cycles to step each dipole family up and down. After this, the orbit-response matrix is inverted by keeping all three singular values.

Figure 5 demonstrates the first two iterations of this correction scheme. The blue curve is the initial orbit corresponding to the red curve in Fig. 4. The red and black curves represent the horizontal orbit after the correction is applied, demonstrating the effectiveness of the method. Potentially, an optimisation procedure might shift the timing of all pulsed magnets to a different local minimum. However, in this case, the correction scheme accurately identified the initial timing offsets. At this step, the BPM readout errors are absent in this simulation. Next, the top panels of Fig. 6 demonstrate the deviation of the betatron tunes throughout the ramp, whilst the bottom panel represents the chromaticity. The left column shows the scenario where no correction is applied, and the right column corresponds to the case when the booster power supplies are synchronised by using the

ORM method. The results demonstrate that the timing error can be minimised.

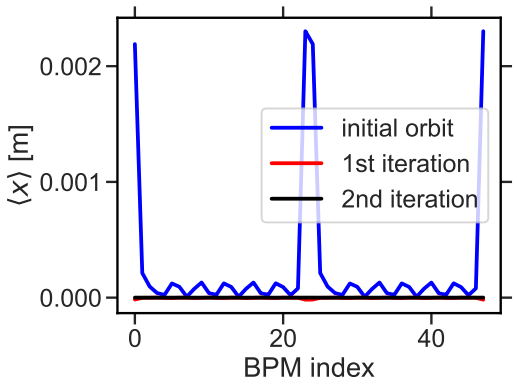

Figure 5: Horizontal orbit at 195 MeV during the optimisation process.

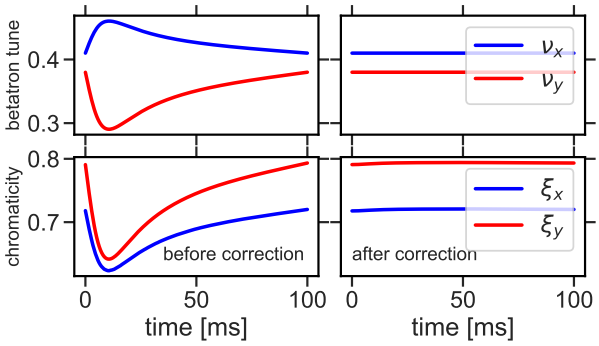

Figure 6: Horizontal and vertical betatron tunes and chromaticity during the ramp, before and after correcting the time synchronisation of booster dipole magnets.

Next Steps

The optimisation procedure above does not include the amplitude and alignment errors in magnets, and it is based on the closed-orbit calculation in AT2. Noise in the turn-by-turn data of the BPMs as well as the time and energy jitter of the injected beam should be included in the correction scheme. Next, the synchronisation errors in quiadrupole and sextupole families have to be included into the analysis.

SUMMARY AND CONCLUSIONS

This work presents the results of particle simulations with realistic multipole errors in quadrupoles and sextupoles based on the magnet measurements, errors in the magnet gradients and eddy-current effects. The dynamic-aperture deviation throughout the ramp is found to be within the acceptable limit, and it is larger than the physical aperture. Next, the synchronisation error of the booster dipole magnets was studied. The results show that the timing error can result in a large closed-orbit deviation, as well as the shift of betatron tunes and chromaticities. Finally, the initial steps in the development of the correction schemes were presented.

REFERENCES

[1] I. P. S. Martin *et al.*, "Progress with the Booster Design for the Diamond-II Upgrade", in *Proc. of International Particle Accelerator Conference (IPAC'21)*, 2021. doi:10.18429/JACoW-IPAC2021-MOPAB071

[2] M. Borland, "Elegant: A Flexible SDDS-Compliant Code for Accelerator Simulation", in *Proc. PAC'00*, Chicago, IL, USA, pp. 2595–2597, 2000. doi:10.2172/761286

[3] "Accelerator Toolbox", https://atcollab.github.io/at/, Accessed: 2026-05-06,